Available online at www.sciencedirect.com
SCIENCE DIRECT
Cement & Concrete Composites 28 (2006) 509–519
Cement & Concrete Composites
www.elsevier.com/locate/cemconcomp

AC-impedance response of multi-walled carbon nanotube/cement composites

S. Wansom, N.J. Kidner, L.Y. Woo, T.O. Mason *

Materials Research Center, Department of Materials Science and Engineering, Northwestern University, 2220 North Campus Drive, Evanston, IL 60208-0001, USA

Accepted 18 January 2006
Available online 22 March 2006

Abstract

AC-impedance spectroscopy (AC-IS) was combined with time-domain reflectometry (TDR) to investigate the impedance response of fiber-reinforced cement (FRC) composites with multi-walled carbon nanotubes (MWCNTs). In Nyquist plots (−imaginary impedance vs. +real impedance) three impedance arcs/features were observed, similar to Nyquist plots for macrofiber and microfiber FRCs. The intersection of the electrode arc and the intermediate frequency feature (R_{DC}(FRC)) corresponds to the DC resistance of the composite. The intersection of the two bulk features (R_{cusp}) corresponds to the AC resistance of the composite. Reductions in (R_{DC}(FRC)) from the matrix resistance are indicative of a nanotube percolating network. Reductions in R_{cusp} from the matrix resistance are indicative of a discontinuous fiber–fiber path. Both shifts increased with fiber loading. AC-IS measurements are therefore able to discriminate percolation vs. discontinuous fiber effects in CNT-FRCs, with the potential for characterizing dispersion issues (e.g., clumping/aggregation) in nanocomposites.

Keywords: Cement-based composites; Nanocomposites; Carbon nanotubes; Impedance spectroscopy; Time-domain reflectometry

1. Introduction

Since their discovery by Iijima in 1991 [1], there has been growing interest in carbon nanotubes (CNTs) for various composite applications owing to their outstanding physical properties. Mechanically, they exhibit elastic moduli in the TPa range [2]. Their exceptionally high theoretical strength is 100 times that of steel, at only 1/6th the specific gravity [3]. Although the exact magnitude of these values depends on the diameter and chirality (how their graphitic sheets are rolled into tubes), and whether they are single-walled or multi-walled, values as high as 60 GPa for ultimate strength and 6% for ultimate strain have been reported (single-walled CNTs [4,5]). Their strength and ultrahigh aspect ratios (length/diameter) make them ideal candidates for reinforcing fibers. Significant gains up to three times in toughness have been reported for CNT/alumina composites [6].

Regarding their electrical properties, single-walled CNTs (SWCNTs) can be semiconducting or metallic in character, depending upon their chirality. Multi-walled CNTs (MWCNTs), on the other hand, are metallic in character. Electrical conductivities on the order of 10^5–10^6 S/cm have been reported for MWCNTs [7]. When used as a conductive filler in polymer matrix composites, the resulting ultralow electrical percolation thresholds are attractive for low-density and cost-sensitive electronic applications. Therefore, there has been prolific literature on CNT–polymer matrix composites in recent years.

However, research activity in the area of carbon nanotube fiber-reinforced cements (CNT-FRCs) has been very limited. Makar and Beaudoin [8] reported briefly on an ethanol/sonication technique for dispersing CNTs in cement, while Campillo et al. [9,10] reported modest gains

* Corresponding author. Tel.: +1 847 491 3198; fax: +1 847 491 7820.
E-mail address: t-mason@northwestern.edu (T.O. Mason).

0958-9465/$ - see front matter © 2006 Elsevier Ltd. All rights reserved.
doi:10.1016/j.cemconcomp.2006.01.014

in compressive strength and nanoindentation hardness for MWCNTs in cement pastes vs. plain pastes. More recently, Li et al. [11] devised a carboxylation procedure to improve the MWCNT–cement matrix bond. They reported only slight improvements in compressive strength and failure strain compared to the unreinforced matrix. The meager gains reported for CNT-FRCs may be due to CNT dispersion issues and/or weak CNT–cement matrix bond. Dispersion problems have been documented for the more widely studied CNT–polymer matrix composites [12].

Our prior work [13–19] has shown that AC-impedance spectroscopy (AC-IS) can be used to characterize the microstructure of fiber-reinforced cements (FRCs) with discontinuous conductive (e.g., carbon or steel) macrofibers (mm-scale diameters) or microfibers (μm-scale diameters). AC-IS has been employed to investigate fiber dispersion issues in macro- and microcomposites, including orientation, coarse-scale segregation, and local aggregation [18]. Of these issues, local aggregation (clumping) should be particularly applicable to CNT-FRCs, as adequate dispersion of carbon nanotubes in cement matrix proves very challenging to achieve.

The present work reports AC-IS measurements for cement-based composites containing MWCNTs. Four-point DC measurements are employed to assist assignment of features in the AC-IS response. Time-domain reflectometry (TDR), a high-frequency dielectric spectroscopy technique, is also employed to extend the practical frequency range to higher frequencies, and thus to resolve some features unattainable by the AC-IS technique. To the authors' knowledge, this is the first report on the AC-IS response of CNT-FRCs. The features obtained are discussed with respect to the well-understood AC-IS response of microcomposites, and whether electrical techniques for characterizing dispersion in macro- and microcomposites can be extended to CNT-FRCs.

2. Experimental procedures

Three different mixes of unreinforced and reinforced cement (0.75 vol% MWCNTs, 1 vol% MWCNTs) were fabricated at a fixed water-to-cement ratio of 0.45 (by weight). MWCNTs were used, as opposed to SWCNTs, because of their higher conductivity. Type I ordinary Portland cement (OPC) was first dry-mixed with methylcellulose (Methocel F4M, Dow Chemicals) in the amount of 0.4% by weight of cement. A polycarboxylate superplasticizer (Catexol Superflux 2000 PC, Axim Italcenti Group) in the amount of 0.5% by weight of cement was added to the mixing water, followed by the MWCNTs (initially 10–20 nm diameter × 1–2 μm length, Helix Material Solutions, TX). The solution was stirred by hand for 2 min and then ultrasonicated for 5 min until the MWCNTs appeared to be well dispersed in the solution. The cement mixture was then added to the solution and hand-mixed for another 2 min, before half of the mix was cast into a polycarbonate mold (12.5 mm × 12.5 mm × 25 mm). For AC-IS measurements, two stainless steel electrodes (12.5 mm × 15 mm × 0.2 mm) were embedded at the two ends of the specimen (25 mm electrode spacing) immediately after casting. The other half of the mix was reserved for TDR measurements (see below), to be taken concurrently with the AC-IS measurements. The unreinforced OPC specimen (with methylcellulose and superplasticizer) was fabricated using the exact same protocol. To test for reproducibility, two more replicates were made for each composition for AC-IS measurements only.

A Solartron 1260 impedance/gain-phase analyzer with Z-60 data collection software (Schlumberger, Houston, TX) was employed for the AC-IS measurements. Two-point AC-IS measurements were made using the embedded electrodes (Fig. 1a) at 15 min, 1 h, 4 h, 6 h and 8 h after mixing. At 1 day, the specimens were demolded and AC-IS measurements were performed using sponges (12.5 mm × 12.5 mm × 2 mm) soaked in aqueous solution (0.33 M KOH + 0.13 M NaOH), which approximates the conductivity of OPC pore solution at early ages, and lightly pressed against stainless steel electrodes (Fig. 1b). Four-point DC measurements, performed only at 1 day, were taken by wrapping stainless steel wires (0.2 mm diameter) at 1/4 and 3/4 positions around the specimens to serve as voltage contacts (Fig. 1c). Current was applied in 0.25 mA increments from 1.5 mA to −1.5 mA across the two pressed-sponge electrodes. The specimen DC resistance (R_{DC}) was calculated from the slope of the current–voltage plot when appropriately corrected for geometry (from $L/2$ to L where L is the specimen length). It should be stressed that the specimens were kept in a moist environment at all times until tested. The excitation amplitude was 1 V over the frequency range from 0.1 Hz to 30 MHz, with data collected at 10 steps per decade of frequency.

For TDR measurements, the specimens were cast into a 10-ml beaker. A coaxial wire (semirigid UT 141, 3.5 mm) was stripped back to expose approximately 5 mm of the inner conductor, which was then inserted into the specimen. A 4 mm × 7 mm castle nut (Slotted/Castlelated Hex Nut #935, Metric and Multistandard Components Corp., Hawthorne, NY) was attached to the outer conductor of the coaxial cable to shield the inner conductor while the slotted top allowed the cement to flow freely. The TDR experimental setup is shown in Fig. 1d. An HP 54120 digitizing oscilloscope with a 54121A TDR sampling head was used to generate a voltage pulse with a very short rise time (20 ps) and to detect the incident and reflected voltage pulse, which includes quantitative dielectric properties of the specimen. Consecutive segments of the TDR reflected transient were analyzed using a variable time scale sampling method. The reflected transient was then transformed into the frequency domain (corresponding to 1 kHz–18 GHz in the present work) using a numerical Laplace transform. To determine the empty cell capacitance of the sampling cell, calibration with standard liquids of known dielectric constant (e.g., acetone, methanol and de-ionized water) was also performed.

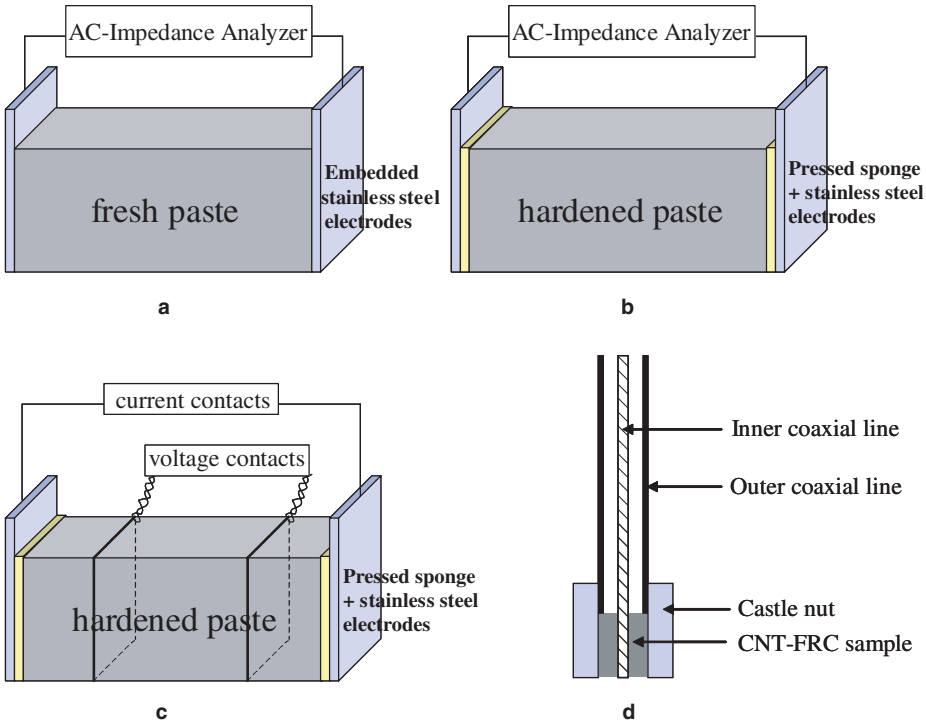

Fig. 1. Experimental setup for (a) AC-IS measurements of fresh CNT-FRCs (15 min up to 8 h), (b) AC-IS measurement of hardened CNT-FRCs (1 day), (c) four-point DC measurements of hardened CNT-FRCs (1 day) and (d) TDR measurements of both fresh and hardened CNT-FRCs.

3. Results and discussion

3.1. Prior results on AC-IS response of microfiber composites

The AC-impedance spectroscopy (AC-IS) technique involves application of AC excitation of set amplitude over a range of frequencies to the specimen. The measured response of the specimen, which includes both magnitude and phase angle, can be represented in a Nyquist plot (negative imaginary impedance, $-\mathrm{Im}(Z)$, vs. real impedance, $\mathrm{Re}(Z)$), with frequency increasing from right to left. The plot contains semicircles or arcs whose diameters correspond to the resistances of the different components in the composite microstructure. Fig. 2 shows a typical Nyquist plot for ordinary Portland cement (OPC) with and without 1 wt.% (~0.06 vol%) carbon microfibers at 7 days of hydration. The fibers were initially 18 mm long by 0.18 μm diameter; however, carbon fibers are known to break up considerably during mixing [16]. Frequency markers (log of frequency in Hz) are shown as darkened points with corresponding numbers. The incomplete rightmost arc, labeled as feature (3), corresponds to the electrochemical response of the external steel electrodes used to take measurements. The key feature of microfiber composite Nyquist plots is the occurrence of two bulk arcs (features (1) and (2) in Fig. 2) vs. a single bulk arc (for unreinforced matrix). Note that the low-frequency cusp (between the electrode arc and the composite bulk arc) coincides with the four-point DC resistance, R_{DC}, of the composite (the solid symbol on the real impedance axis). Furthermore, it remains relatively unchanged (vs. unreinforced OPC) upon the addition of fibers.

The origin of the above dual-arc behavior in FRCs with conductive fibers is explained by the "frequency-switchable coating model" [14,19]. At DC and low AC frequencies, as long as the fiber volume fraction (ϕ) is in the dilute regime and well below the percolation threshold, an electrochemical double-layer (polarization resistance) on fiber surfaces electrically isolates them from the matrix. The fibers behave as if they were insulating at DC and low AC frequencies. Insulating fibers at small volume fraction will have negligible effect on the DC resistance of the composites [16]. At higher AC frequencies, however, displacement currents short out the double layers on the fibers, rendering them conductive (i.e., the fibers become short-circuit current paths through the composite). The marked decrease in resistance (increase in composite conductivity) compared to R_{DC}, as reflected in the high-frequency cusp (R_{cusp}), is a direct result of the conducting fibers.

A more quantitative "universal equivalent circuit model" was developed to describe the impedance response of composites with conducting particulates (i.e., with spheroidal or disc-shaped particles, as opposed to fiber-shaped fillers) or discontinuous fibers in the dilute regime [20]. As shown in Fig. 3, each box represents a resistor and a capacitor in parallel. The uppermost path is the matrix path, with the first element representing the unreinforced matrix. The second element to its right only comes into play in particulate composites, where the addition of particles

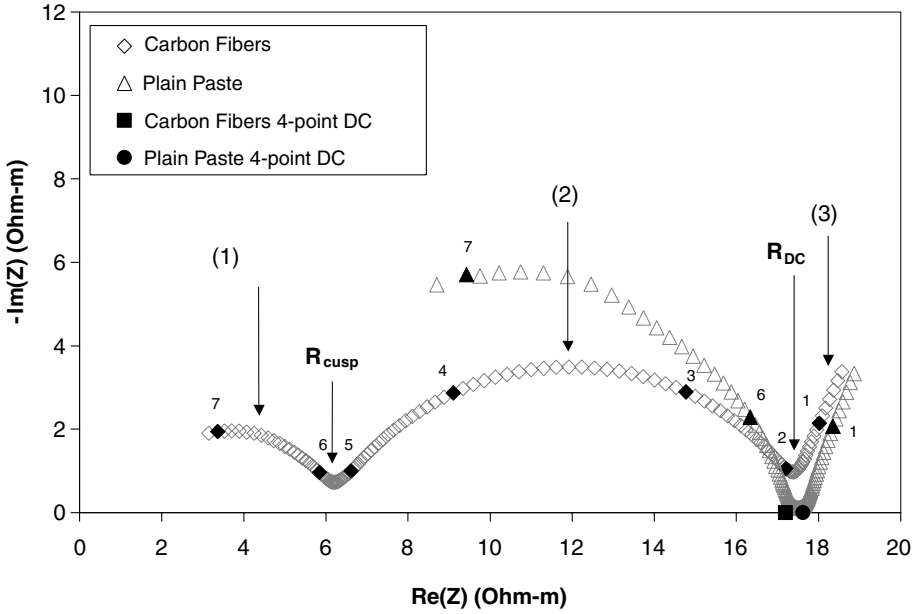

Fig. 2. Typical Nyquist plot at 7 days of hydration for cement with and without 1 wt.% (~0.06 vol%) carbon microfibers. Frequency markers (log of frequency in Hz) are shown as numbers corresponding to darkened points. Four-point DC resistances are shown on the Re(Z) axis.

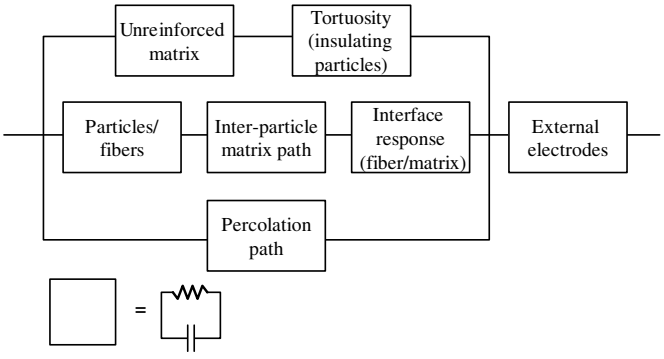

Fig. 3. Schematic of the "universal equivalent circuit model" for particulate and discontinuous (conducting) fiber FRCs. Each box represents a resistor–capacitor combination (in parallel). See text for details.

introduces a tortuosity effect (i.e., insulating particles) at DC and low AC frequencies [17], but is negligible for fiber composites. The middle path is the particle or fiber path, with the first element representing the electrical properties of the particles or fibers. The next element accounts for inter-particle (or inter-fiber) current flow at high frequencies, which is responsible for the decreased resistance at the high-frequency cusp in Fig. 2. This element can be accounted for based upon known mixing laws for particles or the intrinsic conductivity approach (see below) for conducting fibers in the dilute regime. The element to the right side of the middle path represents the polarization resistance/double layer capacitance on the fiber surfaces, just as the rightmost element in Fig. 3 represents the interfacial response for the external electrodes. Although the RC time constants were identical for these two elements, the lumping of the fiber interface RC element with the other elements in the composite vs. the stand-alone RC element for the external electrodes allowed for separation of bulk vs. electrode arcs. Based upon only the upper two paths of the universal equivalent circuit model, excellent agreement between simulated and measured AC-impedance spectra for both particulate and fiber composites has been obtained (see [20] for typical values of the circuit elements). To describe the behavior of FRCs beyond the percolation threshold (see below), the bottom path is required to allow for percolation between particles or fibers, i.e., a continuous electrical path via fibers exists in parallel with that of the matrix [21]. The role of this percolation path will be evident in the DC resistance response of CNT-FRCs discussed in the next section.

An "intrinsic conductivity" approach has been employed in our prior work to characterize the microstructure of cement-based microfiber composites [16]. In the dilute regime, assuming completely random distribution of fibers, the effective conductivity of a composite, $\sigma_{\text{composite}}$, containing fibers of conductivity, σ_{fiber}, and volume fraction, ϕ, suspended in a matrix of conductivity, σ_{matrix}, is described by:

$$\frac{\sigma_{\text{composite}}}{\sigma_{\text{matrix}}} = 1 + [\sigma]_{\Delta}\phi + 0\phi^2, \quad \Delta \equiv \frac{\sigma_{\text{fiber}}}{\sigma_{\text{matrix}}} \tag{1}$$

The first-order coefficient of ϕ in (1) is referred to as the "intrinsic conductivity" and can be calculated for any aspect ratio (length/diameter) of right-cylinder shaped fibers [16]. The higher order terms in ϕ are neglected in the dilute situation. For example, insulating fibers with aspect ratios greater than 10 have an intrinsic conductivity of $-5/3$, regardless of length. Since the product of intrinsic conductivity and volume fraction (ϕ) yields the fractional contribution to the overall composite conductivity, $\phi = 0.0006$ (as in Fig. 2) would result in a mere 0.1% decrease in

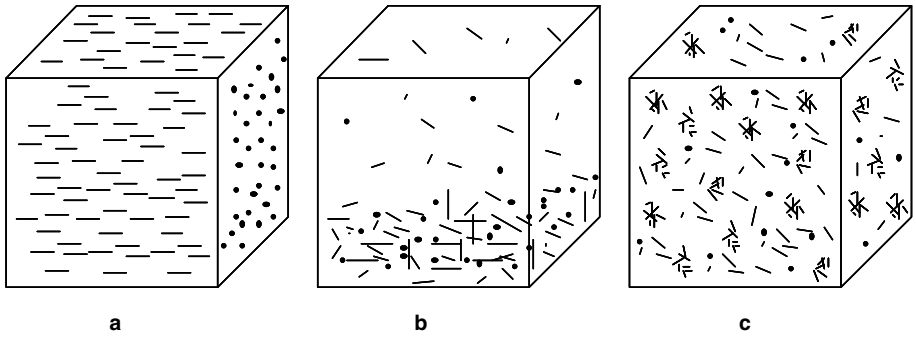

Fig. 4. Schematic of fiber dispersion issues investigated using AC-impedance spectroscopy in FRC macro- and microcomposites, including (a) orientation, (b) coarse-scale segregation and (c) local aggregation. Only local aggregation should be directly applicable to CNT-FRCs.

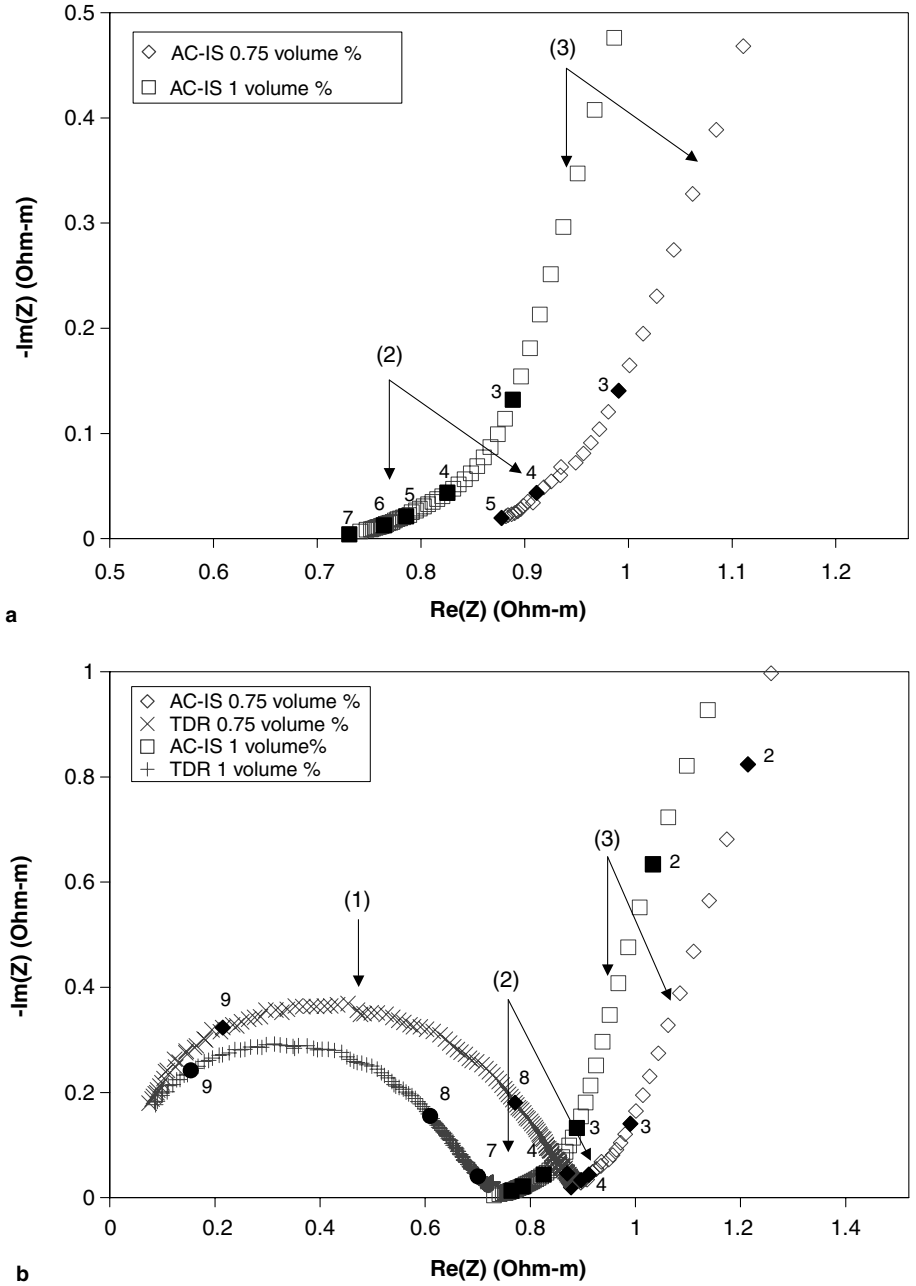

Fig. 5. Experimental Nyquist plots for CNT-FRCs with 0.75 vol% and 1 vol% MWCNTs at 15 min from (a) AC-IS measurements and (b) with TDR measurements superimposed at high frequencies. The two bulk arcs and an electrode arc (features (1), (2) and (3), respectively) are also identified.

conductivity (increase in resistance), which is much less than the typical ±5% uncertainty in AC-IS measurements. This explains why the otherwise conducting fibers have negligible influence on the low-frequency cusp, also referred to as R_{DC} in Fig. 2. It also explains why AC-IS measurements will be insensitive to the presence of truly insulating fibers such as polypropylene. Note that for conducting fibers, the ratio between the fiber and matrix conductivities approaches infinity ($\Delta \to \infty$). Conducting fibers with an aspect ratio of 100, for example, have an intrinsic conductivity of 609, which explains the much higher composite conductivity (lower resistance) at high frequencies in Fig. 2.

The ratio of the composite conductivity (when the fibers are conducting, i.e., at high frequencies) to the matrix conductivity is related to the AC-IS-derived resistances given by (see Fig. 2):

$$\frac{\sigma_{composite}}{\sigma_{matrix}} = \frac{R_{matrix}}{R_{composite}} = \frac{R_{DC}}{R_{cusp}} \tag{2}$$

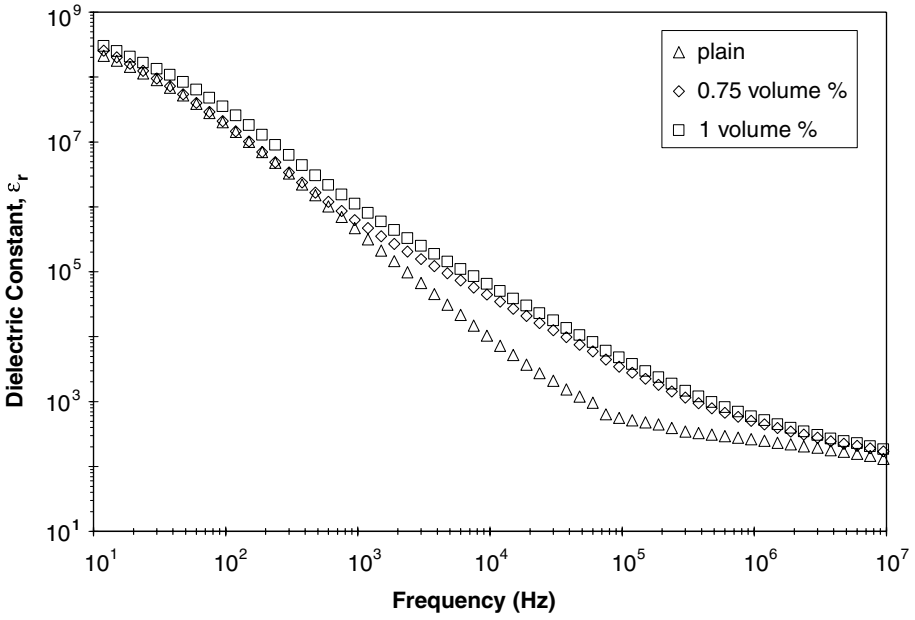

Fig. 6. Dielectric constant vs. frequency plots for plain cement paste and the two composites (with 0.75 vol% and 1 vol% MWCNTs).

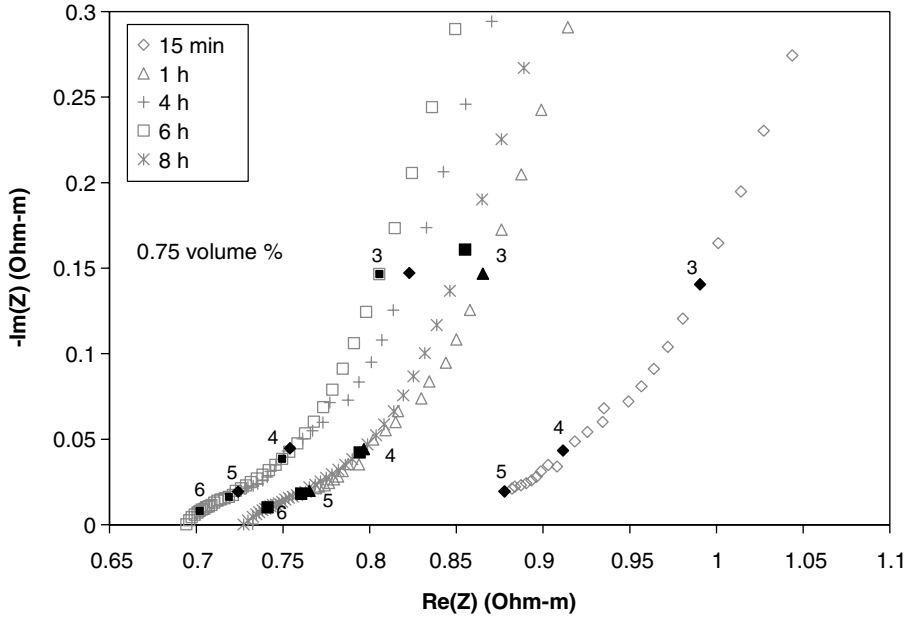

Fig. 7. Experimental Nyquist plots for a CNT-FRC with 0.75 vol% MWCNTs at early times from 15 min to 8 h. Similar response was observed for 1 vol% MWCNTs (not shown).

Combining (1) and (2) and rearranging yields:

$$\text{f-function} = \frac{R_{DC}}{R_{cusp}} - 1 = [\sigma]_{\infty}\phi \quad (3)$$

This "f-function" represents the overall contribution of fibers to the composite conductivity. It has been employed in our prior work to explore fiber dispersion issues in FRC macro- and microcomposites, including orientation, coarse-scale segregation, and local aggregation, which are depicted in Fig. 4 [18]. It should be stressed that, among these issues, only local aggregation will be readily applicable to CNT-FRCs. The other two issues (orientation, segregation) may be more difficult to quantify for CNT-FRCs, given the complexity of nanofiber morphology in comparison with rigid macro- or microfibers.

3.2. Carbon nanotube-reinforced cements or concretes (CNT-FRCs)

Fig. 5a shows the experimental Nyquist plots for CNT-FRCs with 0.75 vol% and 1 vol% MWCNTs at 15 min. (Each specimen was from the same mixing batch as that used in the concurrent TDR measurements, as is the case for Figs. 5–10). The low-frequency bulk arc and the

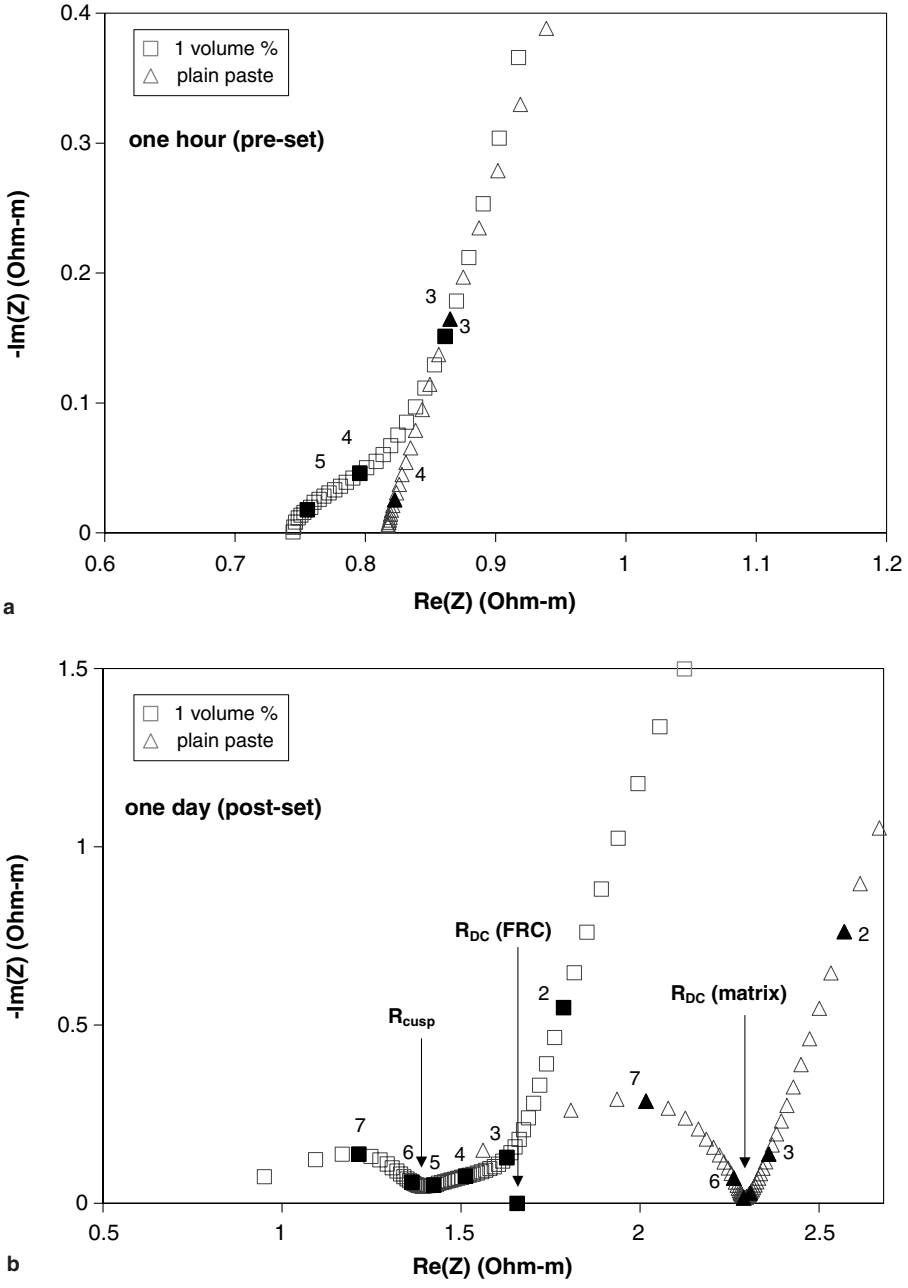

Fig. 8. Nyquist plots for cement paste with and without 1 vol% MWCNTs at (a) 1 h after mixing and (b) 1 day after mixing. The three parameters including R_{cusp}, R_{DC}(FRC) and R_{DC}(matrix) are shown at 1 day.

electrode arc (features (2) and (3), respectively) are evident in each case. The high-frequency bulk arc cannot be resolved by AC-IS measurements in fresh paste due to parasitic inductive contributions in the high-frequency range. With the TDR measurements superimposed onto the AC-IS results at high frequencies, as shown in Fig. 5b, the high-frequency bulk arc (feature (1)) is now evident for both volume fractions. Furthermore, there appears to be a direct mapping of features between CNT-FRCs and microcomposite response (see Fig. 2), even as early as 15 min after mixing (except for the shape of the CNT-FRCs low-frequency bulk arc). The intersection of the low-frequency bulk arc and the electrode arc is an indication of the DC resistance of the CNT-FRCs, as is the case for microcomposites (referred to as R_{DC} in Fig. 2) and post-set CNT-FRCs (referred to as R_{DC}(FRC), see below).

It should be noted that a similar intermediate-frequency feature in Nyquist plots was observed by McCarter et al. in cement pastes with fly ash additions [22]. They attributed a flattened arc/feature at intermediate frequencies to the carbon content of the fly ash. Furthermore, they observed an enhancement of dielectric constant at intermediate frequencies with increasing fly ash/carbon content. A similar phenomenon was observed in the present work. Fig. 6 shows dielectric constant vs. frequency plots for the plain paste and the two composites. The presence of fibers clearly enhances the dielectric constant in the 10^3–10^6 Hz range above the baseline dielectric constant of the paste. (The baseline dielectric constant of the plain paste is ~300 and significantly larger than the dielectric constant of water (~80). This enhancement has been attributed to polarization phenomena within the C–S–H gel phase [23].)

Fig. 7 shows AC-IS Nyquist plots for a CNT-FRC with 0.75 vol% MWCNTs from 15 min to 8 h. Based on the intersection of the low-frequency bulk arc and the electrode arc, the plots show a trend toward lower DC resistances over 15 min–6 h, which is consistent with the release of ions into solution to participate in the hydration reaction. At longer times (e.g., 8 h), ions are consumed to form the hydration products, including calcium silicate hydrate or C–S–H (i.e., the specimens start to set), and the plots show a shift back toward high resistance. The evidence of set thus appears to be between 6 and 8 h for the 0.75 vol%. A similar response was observed for 1 vol% MWCNTs (not shown).

Fig. 8 shows the evolution of AC-IS features from initial casting through set of the 1 vol% MWCNT specimen in comparison to the unreinforced matrix (plain paste). At 1 h (pre-set), the intermediate-frequency feature is already present in the CNT-FRC (Fig. 8a) and the position of the electrode arc of the CNT-FRC is virtually identical to that of the plain paste specimen. By 1 day (post-set), the Nyquist plot for the 1 vol% specimen in Fig. 8b shows three features, similar to the corresponding response for the microcomposite (except for the shape of the intermediate-frequency feature, in contrast to a clear arc shape in Fig. 2). The depressed high-frequency arc at 1 day (owing to parasitic inductive effects in the MHz frequency range) is better resolved by TDR, as shown with the TDR data superimposed at high frequencies in Fig. 9. This also confirms the location of the high-frequency cusp, R_{cusp}, associated with the discontinuous fiber effect in FRCs (as opposed to the percolative fiber effect, see below).

The location of the DC resistance (R_{DC}(FRC), measured only at 1 day) on the Re(Z) axis in Fig. 9 allows for the electrode response to be identified. Note also that the AC-IS cusp of the plain paste in Fig. 8b agrees with the DC resistance of the plain paste, R_{DC}(matrix), in Fig. 9.

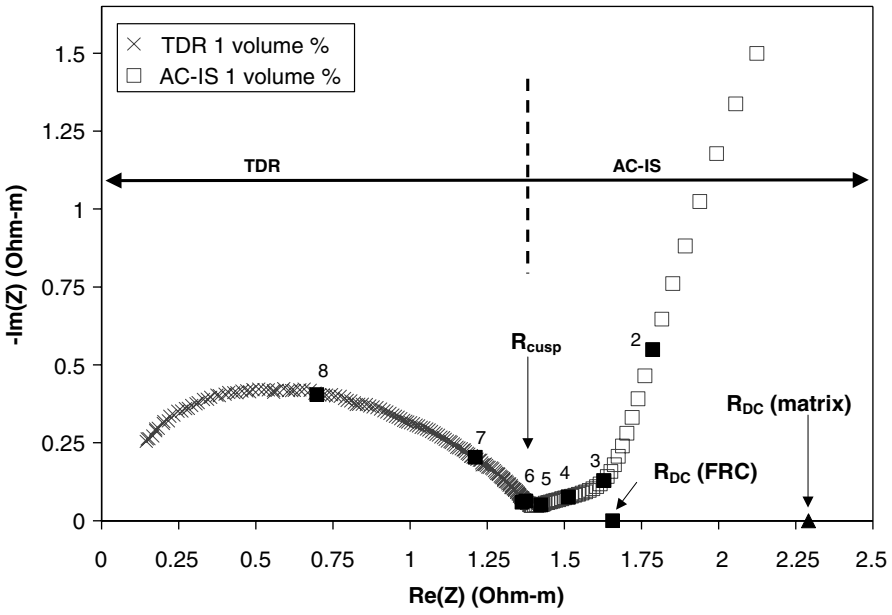

Fig. 9. Nyquist plot for CNT-FRC containing 1 vol% MWCNTs at 1 day with TDR data superimposed on the AC-IS data at high frequencies. The R_{DC}(matrix) shown here (from four-point DC measurements) corresponds to the AC-IS cusp of the plain matrix shown in Fig. 7b.

At 1 day (post-set), the electrode arc is clearly shifted relative to that of the plain OPC specimen; there is a marked decrease in the DC resistance of the composite, R_{DC}(FRC) vs. that of the matrix, R_{DC}(matrix), as shown in Fig. 8b. (The same behavior is also observed in the 0.75 vol% specimen, shown in Fig. 10. However, the shift is more dramatic in the case of the 1 vol% specimen, as expected.) This is a major difference from microcomposite and macrocomposite behavior, where the composite's DC resistance remains essentially unchanged vs. that of the unreinforced matrix (see Fig. 2) [15]. Our interpretation for the shift in DC resistance of the CNT-FRCs is that the percolation path in the equivalent circuit of Fig. 3 is making its presence felt in the DC conductivity (resistance). Whereas there are two important parameters in the AC-IS response of macro- and microcomposites (R_{DC} and R_{cusp} in Fig. 2), there are now three important parameters in the AC-IS response of CNT-FRCs (R_{cusp}, R_{DC}(FRC), and R_{DC}(matrix) in Figs. 8b and 10b). Using these parameters, one can potentially separate the influence of percolation (R_{DC}(FRC)) from that of discontinuous fibers (R_{cusp}) in CNT-FRCs.

The percolation transition in nanofiber composites will be substantially more gradual than that in microfiber and macrofiber composites. A single nanostrand, for example, from one electrode to the other in a

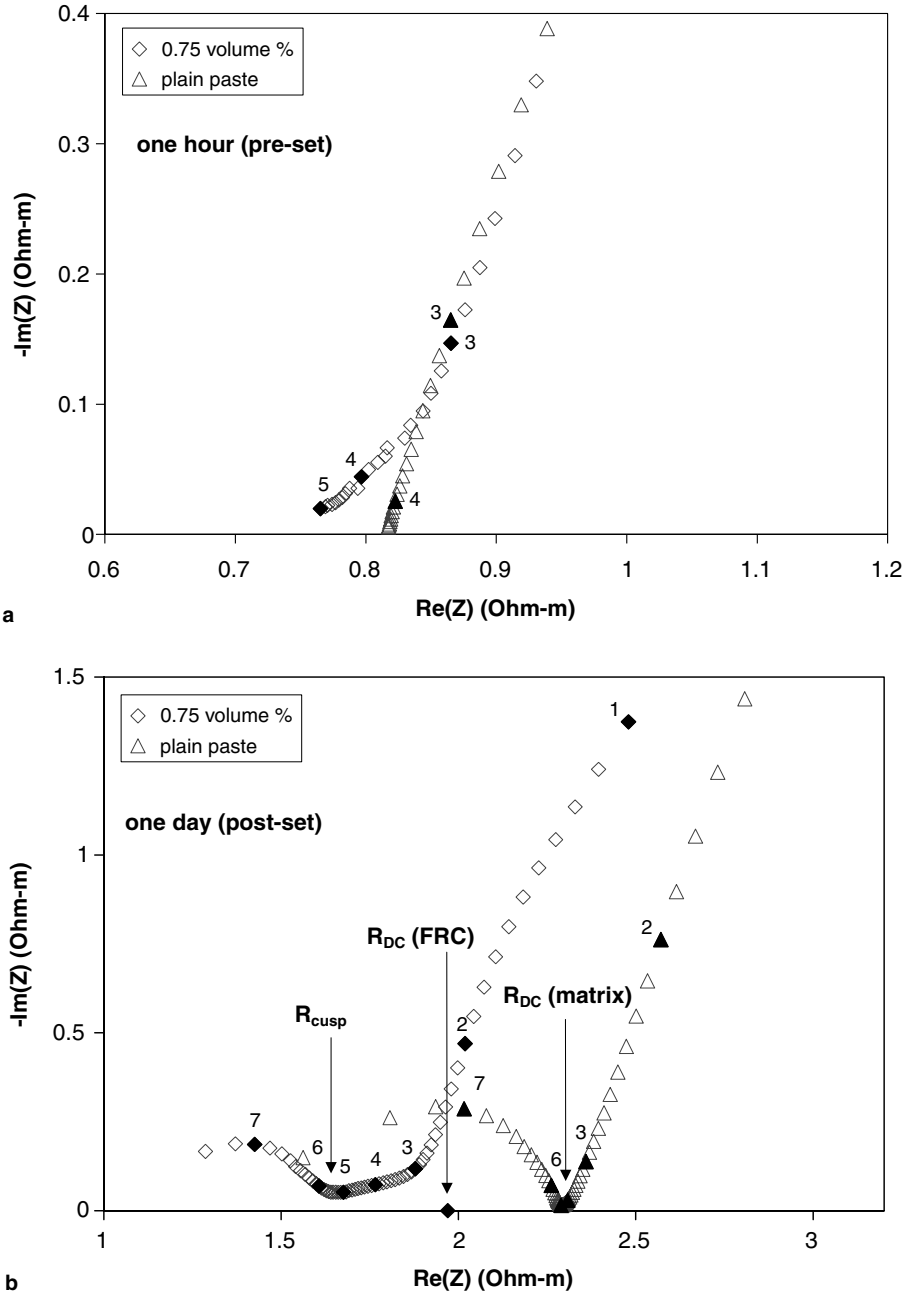

Fig. 10. Nyquist plots for cement paste with and without 0.75 vol% MWCNTs at (a) 1 h after mixing and (b) 1 day after mixing.

1.25 cm × 1.25 cm × 2.5 cm specimen (based upon a fiber conductivity of 10^6 S/cm [7]) will have a resistance in the MΩ range compared to hundreds of ohms for the pre-set cement matrix. For this calculation, a nanotube diameter of ~20 nm was assumed. As a result, the upper matrix path in the equivalent circuit of Fig. 3 dominates the DC and low-frequency AC response of the pre-set CNT-FRCs. This explains why there is no difference between the CNT-FRCs and the plain paste DC resistance at 1 h. By 1 day (post-set), however, the noticeable increase in composite DC conductivity (decrease in resistance) vs. that of the plain paste suggests that the percolation path is now playing an important role. Current now travels through the CNT-FRCs by both the matrix and the percolation paths in the equivalent circuit, resulting in a DC resistance lower than that of the matrix alone. This behavior can be attributed to the decrease in the matrix conductivity (increase in resistance) by an order of magnitude in going through set, allowing for the percolation path to make a noticeable contribution to composite conductivity. Based upon the parallel fiber percolation and matrix paths, the conductivity (resistance) of the matrix (post-set), and the conductivity (resistance) of an individual nanostrand, one can estimate the number of percolation paths spanning the electrodes to be on the order of hundreds.

Fig. 11 shows Nyquist plots based on point-by-point average of three replicates (i.e., average of three Re(Z) and $-$Im(Z) values for each frequency) for each composition. The corresponding DC resistances, averaged over three replicates, are also shown on the Re(Z) axis. (The reproducibility of the DC resistances among the three replicates for each composition is within 13%.) The trends in R_{DC}(FRC) and R_{cusp} compared to R_{DC}(matrix) are similar for both fiber loadings. The decrease in R_{DC} (to R_{DC}(FRC) from R_{DC}(matrix)) for the 1 vol% specimens is larger than the decrease in R_{DC} for the 0.75 vol% specimens, consistent with a more extensive percolating network of nanotubes in the more highly loaded composite. Similarly, the decrease from R_{DC}(matrix) to R_{cusp} for the 1 vol% specimens is larger than that for the 0.75 vol% specimens. This larger decrease is consistent with a larger f-function in Eq. (3), corresponding to a greater influence of the middle fiber–matrix–fiber path (Fig. 3) for the more highly loaded composite.

This suggests that AC-IS has the potential to discriminate percolation effects from discontinuous fiber effects in CNT/cement composites. Ongoing work is addressing the possibility of characterizing fiber dispersion issues in CNT-FRCs, especially clumping or aggregation, by AC-impedance spectroscopy.

4. Conclusions

The first experimental AC-IS Nyquist plots for CNT-FRCs at 0.75 vol% and 1 vol% show a trend toward decreasing DC resistances at early times (owing to a release of ions to participate in hydration reaction) and a shift back toward higher DC resistances at later times (reflecting the initiation of set between 6 and 8 h). Pre-set, the agreement in DC conductivity of the CNT-FRCs and the matrix is the result of current traveling through the matrix only (i.e., the resistance of the matrix path is much less than that of the percolating fiber path pre-set).

At 1 day of hydration, the Nyquist plot shows two composite bulk arcs and an electrode arc, similar to the microcomposite response, except for the shape of the

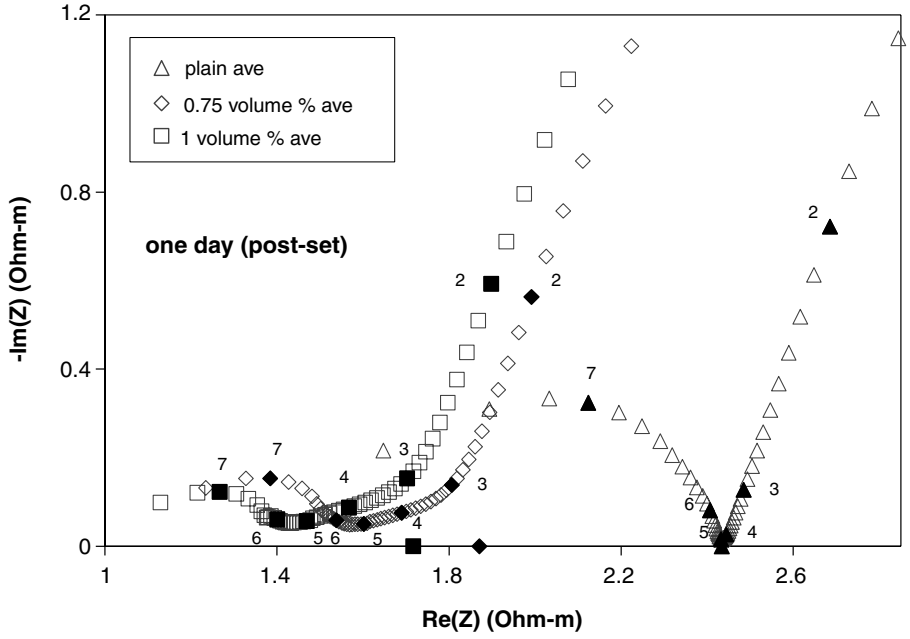

Fig. 11. Nyquist plots for plain cement paste and the two composites (with 0.75 vol% and 1 vol% MWCNTs) based on point-by-point average (for each frequency) over three replicates for each composition.

low-frequency bulk arc. Three important parameters, R_{cusp} (confirmed by TDR), R_{DC}(FRC) (confirmed by four-point DC measurements) and R_{DC}(matrix) can be identified. The noticeable decrease in the DC resistance of the composite from that of the matrix, i.e., $R_{DC}(FRC) < R_{DC}(matrix)$, is a major difference from microcomposite behavior where the two DC resistances remain essentially the same. Such decrease in the DC resistance is attributable to the percolation path in the equivalent circuit. With the increase in the matrix DC resistance by an order of magnitude in going through set, current now travels through the CNT-FRCs via both the matrix and the percolation paths in the equivalent circuit, yielding a DC resistance lower than that of the matrix alone. Using these three parameters from AC-IS measurements, one can differentiate percolation contributions from discontinuous nanotube contributions to the AC-IS response of carbon nanotube cement composites.

Acknowledgement

This work was supported by the National Science Foundation under Grant No. DMR-00-73197 and made use of facilities of the Center for Advanced Cement-Based Materials.

References

[1] Iijima S. Helical microtubes of graphitic carbon. Nature 1991;354(7):56–8.
[2] Salvetat JP, Bonard JM, Thomson NH, Kulik AJ, Forro L, Benoit W, et al. Mechanical properties of carbon nanotubes. Appl Phys A 1999;69(3):255–60.
[3] Wong EW, Sheelan PE. Nanobeam mechanics: elasticity, strength, and toughness, of nanorods and nanotubes. Science 1997;22:161–7.
[4] Yu MF, Lourie O, Dyer MJ, Moloni K, Kelly TF, Ruoff RS. Strength and breaking mechanism of multiwalled carbon nanotubes under tensile load. Science 2000;287:637–40.
[5] Walters DA, Ericson LM, Casavant MJ, Liu J, Colbert DT, Smith KA, et al. Elastic strain of freely suspended single-wall carbon nanotube ropes. Appl Phys Lett 1999;74(25):3803–5.
[6] Zhan GD, Kuntz JD, Wan J, Mukherjee AK. Single-wall carbon nanotubes as attractive toughening agents in alumina-based nanocomposites. Nature Mater 2003;2(1):38–42.
[7] Ebbesen TW, Lezec HJ, Hiura H, Bennett JW, Ghaemi HF, Thio T. Electrical conductivity of individual carbon nanotubes. Nature 1996;382(4):54–6.
[8] Makar JM, Beaudoin JJ. Carbon nanotubes and their application in the construction industry. In: Bartos PJM, Hughes JJ, Trtik P, Zhu W, editors. Nanotechnology in construction. Proceedings 1st international symposium on nanotechnology in construction. Royal Society of Chemistry; 2004. p. 331–41.
[9] Campillo I, Dolado JS, Porro A. High-performance nanostructured materials for construction. In: Bartos PJM, Hughes JJ, Trtik P, Zhu W, editors. Nanotechnology in construction. Proceedings 1st international symposium on nanotechnology in construction. Royal Society of Chemistry; 2004. p. 215–25.
[10] Saez de Ibarra Y, Gaitero JJ, Campillo I. Analysis by atomic force microscopy of the effects of the nanoindentation hardness of cement pastes by the introduction of nanotube dispersions. TNT-2005 Conference, Oviedo, Spain, August 29–September 2, 2005.
[11] Li GY, Wang PM, Zhao X. Mechanical behavior and microstructure of cement composites incorporating surface-treated multi-walled carbon nanotubes. Carbon 2005;43:1239–45.
[12] Martin CA, Sandler JKW, Shaffer MSP, Schwarz MK, Bauhofer W, Schulte K, et al. Formation of percolating networks in multi-wall carbon–nanotube–epoxy composites. Compos Sci Technol 2004;64:2309–16.
[13] Ford SJ, Shane JD, Mason TO. Assignment of features in impedance spectra of the cement-paste/steel system. Cem Concr Res 1998;28(12):1737–51.
[14] Torrents JM, Mason TO, Peled A, Shah SP, Garboczi EJ. Analysis of the impedance spectra of short conductive fiber-reinforced composites. J Mater Sci 2001;36(16):4003–12.
[15] Mason TO, Campo MA, Hixson AD, Woo LY. Impedance spectroscopy of fiber-reinforced cement composites. Cem Concr Comp 2002;24:457–65.
[16] Hixson AD, Woo LY, Campo MA, Mason TO, Garboczi EJ. Intrinsic conductivity of short conductive fibers in composites by impedance spectroscopy. J Electroceram 2001;7:189–95.
[17] Campo MA, Woo LY, Mason TO. Frequency-dependent electrical mixing law behavior in spherical particle composites. J Electroceram 2002;9(1):49–56.
[18] Woo LY, Wansom S, Mason TO, Ozyurt N, Mu B, Shah SP. AC impedance spectroscopy for nondestructive evaluation of fiber-reinforced cement composites. In: Banthia N, Uomoto T, Bentur A, Shah SP, editors. Construction materials: performance, innovations and structural implications and mindess symposium. Proceedings 3rd international conference, 2005.
[19] Torrents JM, Mason TO, Garboczi EJ. Impedance spectra of fiber-reinforced cement-based composites: a modeling approach. Cem Concr Res 2000;30(4):585–92.
[20] Woo LY, Wansom S, Hixson AD, Campo MA, Mason TO. A universal equivalent circuit model for the impedance response of composites. J Mater Sci 2002;38:2265–70.
[21] Ingram BJ, Mason TO. Powder–solution-composite (PSC) electrical conductivity measurement technique for ceramic powder systems. J Electrochem Soc 2003;150(8):E396–402.
[22] McCarter WJ, Starrs G, Chrisp TM. The complex impedance response of fly-ash cements revisited. Cem Concr Res 2004;34(10):1837–43.
[23] Ford SJ, Hwang J-H, Shane JD, Olson RA, Moss GM, Jennings HM, et al. Dielectric amplification in cement pastes. Adv Cem Bas Mater 1997;5:41–8.